19PFL-0866

A Quasi-Dimensional Model of Pre-Chamber Spark-Ignition Engines

Author, co-author (Do NOT enter this information. It will be pulled from participant tab in MyTechZone)

Affiliation (Do NOT enter this information. It will be pulled from participant tab in MyTechZone)

Abstract

Increasingly stringent pollutant and CO_2 emission standards are inducing the car manufacturers to investigate innovative solutions to further improve fuel economy of their fleets. Some of these solutions focus on the vehicle/engine interaction, such as the powertrain electrification, while other techniques directly address thermal efficiency improvements of the engine.

Among them, concerning the spark-ignition engines, an extremely lean combustion shows the potential to reduce the noxious emission and the fuel consumption. However, this approach involves some special challenges, such as ensuring sufficient combustion stability and realizing a new efficient exhaust aftertreatment system, since application of standard three-way catalysts is no longer an option.

A pre-chamber ignition system represents an interesting solution to overcome the combustion stability issue and simultaneously further improve the thermal efficiency. Especially for an active system, with direct fuel introduction into the pre-chamber, a favorable air/fuel mixture ignitability and an adequate combustion speed can be obtained, even with very lean mixtures.

In this work, the combustion characteristics of an active pre-chamber system were investigated with a single-cylinder SI research engine. Conventional gasoline fuel was injected into the main chamber, while the pre-chamber was fed with compressed natural gas. In a first stage, an experimental campaign was carried out at various speeds, spark timings and air-fuel ratios. Global engine operating parameters as well as pressure traces, inside the main combustion chamber and the pre-chamber, were recorded and analyzed.

Using the experimental data, a phenomenological model of this unconventional combustion system with divided combustion chambers has been developed and validated. The model was then implemented in a 1D code. The proposed numerical approach shows the ability to simulate the experimental data with good accuracy using a fixed constant tuning set. The model can correctly describe the behavior of a pre-chamber combustion system under different operating conditions and it is capable to capture the physics behind such innovative combustion system concept.

Introduction

The problem of atmospheric air pollution, caused by the Internal Combustion Engines (ICEs), has never been greater than today. Car manufacturers, driven by more and more stringent legislations, are continuously forced to find proper technical solutions to deal with this issue, without giving up to high-standard engine performance.

The worldwide diffusion of pure electric or Fuel Cell vehicles is a possible scenario, which is also related to the availability of electricity or hydrogen, both produced from renewable energy sources [1,2].

Nevertheless, ICEs are expected to still remain the core component of automotive propulsion systems in the years to come. A wider diffusion of Hybrid Electric Vehicles (HEVs) is also awaited, since they represent the most promising short-term solution to afford next CO_2 emission standards. Further efforts however still need to be focused on the efficiency and pollution improvement of future ICEs, in the medium-long term.

Various solutions for efficiency improvement have already been proposed during last years. Concerning Spark-Ignition (SI) engines, high efficiency downsized and VVA engines [3] have been introduced on the market. Additional benefits are expected from advanced anti-knock measures, as variable compression ratio [4], cooled Exhaust Gas Recirculation (EGR) [5], and water injection [6].

A further step on engine efficiency improvement can be obtained by a very lean air/fuel mixture [7], which is very beneficial also for noxious emission reduction [8]. Improved fuel consumption mainly derives from reduced heat losses and improved knock resistance. A lean mixture, furthermore, leads to significantly decreased NO_X emission, due to a lower burned gas temperature. If neatly burned, an extremely lean air/fuel mixture also guarantees the practical absence of CO and HC emissions.

However, common SI-ICEs can only work in a narrow range of excess of air, reducing the real benefit of this technique. Excess-air must be limited to maintain efficient mixture ignitability and high combustion stability. Over a certain dilution, indeed, combustion speed is extremely reduced, leading to unacceptable cyclic variability and misfire. HC-CO formation moreover rapidly increases [9,10].

The employment of a Pre-Chamber (PC), characterized by a small volume (usually 1%-5% of the clearance volume) and connected with the Main-Chamber (MC) through one or more orifice, can significantly extend the lean burn limit, respect to a conventional SI engine [11,12]. In such system, the combustion process starts at the spark plug located in the pre-chamber. Due to the pressure increment, a turbulent jet of hot gases penetrates the main-chamber, increases the turbulence, and ignites the lean mixture on multiple sites. As a consequence, the burn rate enhances, improving the combustion stability even for extremely lean mixtures.

In a passive system, unburned air/fuel mixture, at the same excess-air of the main chamber, is pushed inside the pre-chamber during the compression stroke. Alternatively, an additional injector can be

located in the pre-chamber (active system) to directly control the local air/fuel ratio. The former solution has the advantage of a low cost and engineering simplicity. The latter is particularly attractive due to the possibility to further extend the lean limit, with still reasonable cyclic variations [11,12,13].

Nowadays, various experimental activities have been reported in the current literature, showing the potentiality of an active pre-chamber in reducing the NO_X emissions, extending the lean limit and improving thermal efficiency [14,15]. To get better mixture formation in an active pre-chamber, gaseous fuels, such as methane [16] and hydrogen [17], or vaporized gasoline [18] have been widely investigated. However, considering the vehicle infrastructure of passenger cars, the liquid gasoline injection into the pre-chamber remains the most suitable option, although some risk of a not-perfect mixture formation and the related soot emissions must be faced.

Numerical studies are also available in the literature, aiming at the development and optimization of a pre-chamber ignition system. Analyses are mainly based on the employment of 3D CFD codes, which appear to be the most suitable approach to well-describe the interaction between combustion, chemical kinetics, and turbulence [19,20,21]. Due to the complexity of involved phenomena and to CPU time requirements, available 3D results are usually limited to a reduced number of operating points.

In the authors' knowledge, a predictive phenomenological model, trying to describe the basic physics behind a divided-chamber engine, is still missing in the current literature. Some preliminary approaches are being developed only in recent years. In [22], turbulent (K-k-ε) and heat transfer models have been proposed for a passive pre-chamber. They are able to reproduce with accuracy 3D reference results, in terms of pressure traces and related turbulence variables. However, the study is limited to the analysis of the compression stroke, due to the absence of a coupling with a combustion model. Differently, in [23], a Wiebe function is imposed to describe the combustion processes in both the chambers, while the heat transfer is evaluated by an authors' correlation. The model is validated trough a comparison with the pressure trace in the main-chamber in a single operating condition. The main drawback is the need to impose a heat release rate derived from experiments, losing the predictive capability of the model.

In this work, indeed, a more comprehensive quasi-dimensional modeling framework is developed, where all basic phenomena occurring in an active PC engine are modeled, such as mixture preparation, turbulence evolution, flame area enhancement, burn rate development, etc. The present research is supported by a European H2020 project (EAGLE: https://h2020-eagle.eu/), having the objective of investigating and developing this novel engine architecture for a HEV, by integrated experimental and numerical activities.

The paper is organized as follows: firstly, the experimental setup and tests of the examined Single Cylinder Engine (SCE) will be briefly described. The SCE is equipped with an active pre-chamber fueled with Compressed Natural Gas (CNG), while liquid gasoline is directly injected in the main-chamber. Subsequently, the quasi-dimensional model for a divided chamber engine will be presented in detail, with focus on the combustion description. Finally, the model will be validated against the experimental results, in terms of pressure traces, combustion development and overall performance. From the experimental campaign, 13 representative operating points have been selected with the aim to assess model sensitivity to the engine speed and relative air/fuel ratio (λ) variations.

Experimental setup and tests

The experimental testing was conducted on a homogeneously operated, direct injection, research SCE at the Institute for Combustion Engines (VKA) of the RWTH Aachen University. The existing base engine features high peak pressure capability, external boosting up to 4 bar and a realization of variable compression ratios by different piston designs. For the investigations of the EAGLE project, a new top-end has been designed. The main engine specifications are listed in Table 1.

Table 1.Engine main features.

Pre-chamber engine	
Bore, mm	75
Stroke, mm	90.5
Stroke / Bore Ratio	1.206
Displacement, cm^3	399
Peak pressure capability, bar	170
Geometrical compression ratio	13
Injection system	Lateral solenoid, 350 bar
Fuel in main-chamber	DI injector, gasoline RON 98
Fuel in pre-chamber	DI injector, CNG
Pre-chamber volume mm^3	~ 1000
$V_{pre\text{-}chamber}$ / V_{TDC}	~ 3 %
Pre-chamber holes	4 - two pairs of different hole size
$A_{jet\ holes}$ / $V_{pre\text{-}chamber}$, cm^{-1}	~ 0.03

The long stroke of 90.5 mm and the arrangement of the valves, combined with the intake port and the combustion chamber shape, generate a charge motion level, which is comparable to state-of-the-art turbocharged engines. Figure 1 shows the SCE engine design. The engine has been operated with a Direct Injection (DI) system at 350 bar and is equipped with a CFD-optimized 4-hole pre-chamber, Figure 1d. The layout process and further results of this pre-chamber have been presented in [14].

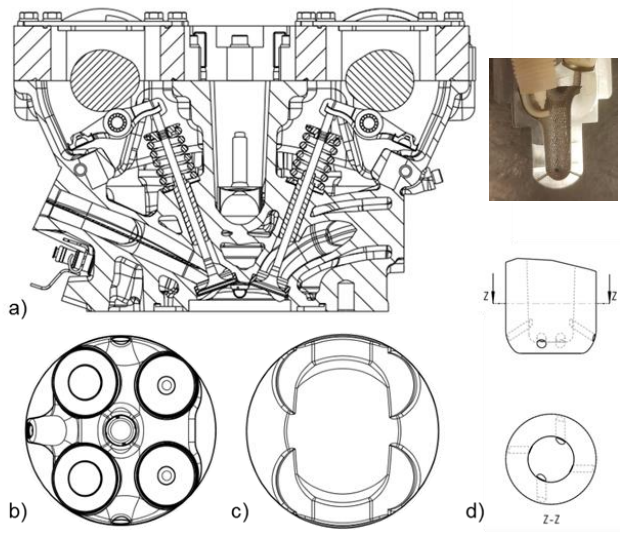

Figure 1. Research engine layout: a) sectional view of cylinder head b) combustion chamber dome c) piston crown for CR=13, d) pre-chamber.

The pressure measurements were carried out as follows:

- for the cylinder, two Kistler A6045 B pressure transducers were employed, flush-mounted in the combustion chamber side roof;
- for the pre-chamber, one Kistler 6054 BR pressure transducer was employed flush mounted in the pre-chamber volume;

- sampling was performed via Kistler charge amplifiers and a FEV combustion analysis system at a resolution of 0.1 CAD;
- for the dynamic intake and exhaust gas pressures, the Kistler 4045 A5 pressure transducers were chosen, with a sampling resolution of 1 CAD.

In total, 500 consecutive cycles were collected. An average of these cycles has been considered for the comparison with the model. Measurements of static pressures and temperatures were performed by conventional pressure transducers and thermocouples during an averaging interval of 30 s. Oil and water conditioning systems allowed for steady-state operations.

For all results shown, the engine was operated under the same Spark Advance (SA) strategy. A preliminary SA sweep has shown that the commonly used combustion phasing (MFB_{50} timing at 7-8 CAD AFTDC) is also the optimum for engine efficiency at ultra-lean operating conditions with the presented pre-chamber. Therefore, the spark advance was set for optimal MFB_{50}, if there was no knocking limitation which required a retarded ignition timing.

The intake air was conditioned to 30 °C in the intake runner. The pressure upstream of the throttle flap and in the exhaust manifold was controlled to 1.01 bar during throttled operation. For boosted operation, the pressure in the exhaust system was set equal to the pressure in the intake manifold. The relative air-fuel ratio of the exhaust gas was derived according to the formula of Spindt [24].

For model development and validation, 13 representative cases, listed in Table 2, are selected from the overall experimental campaign. Three different λ sweeps at constant load are chosen at various engine speeds. In this way, the model predictive capability will be checked by varying the mixture composition from stoichiometric to very lean, with different turbulence levels. From the MFB_{50} values listed in the table, it is evident that almost all cases are knock-limited.

Table 2. List of investigated operating points

Case	Operating condition rpm @ IMEP	λ	SA CAD AFTDC	MFB_{50} CAD AFTDC
1	2000 rpm @ 15 bar	1.0	14.9	33.2
2		1.4	6.8	25.6
3		1.8	-3.4	16.7
4		2.0	-7.5	14.2
5		2.4	-17.2	9.8
6	3000 rpm @ 13 bar	1.0	5.8	23.6
7		1.4	0.3	20.3
8		1.8	-12.2	9.1
9		2.0	-16.9	7.8
10		2.2	-21.0	7.8
11	4000 rpm @ 16 bar	1.0	11.4	33.7
12		1.4	5.7	32.2
13		1.6	2.3	35.2

Engine model description

Mass exchange between pre-chamber and main-chamber – The tested engine architecture is geometrically schematized as two Zero Dimensional (0D) volumes, connected by an orifice. The PC volume is described as a cylinder having the same (constant) volume of the real device. It is connected to the variable volume of the MC through an orifice, having the same equivalent cross-section of the real four-hole geometry. A constant discharge coefficient is selected to describe flow losses in the passage. Mass and energy equations are solved in both volumes and a classical filling-emptying approach is applied to compute mass exchange between them, based on the pressure difference, orifice area and discharge coefficient.

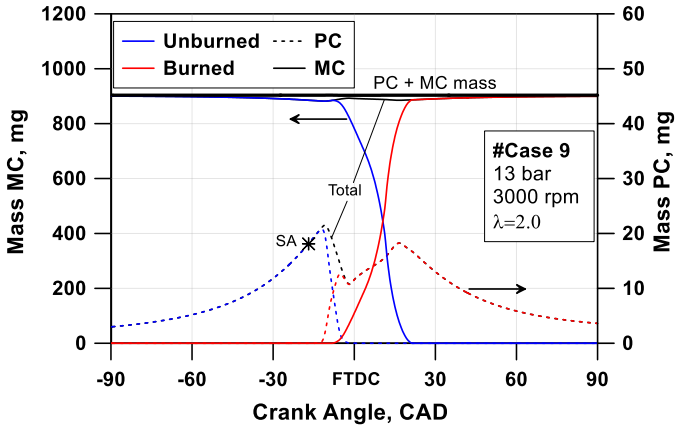

Figure 2. Mass evolution of the unburned and burned gases in the PC and MC.

Figure 2 highlights the mass evolution in both PC and MC, together with their unburned and burned contributions, along the combustion progress. The total mass in the PC increases during the compression stroke, while the corresponding mass in the MC slightly decreases. The overall mass inside the cylinder, computed as the sum of PC and MC contents, is also reported in thick black line, to verify its conservation during the closed valve period (no blow-by).

Another issue concerns the composition of mass exchange between PC and MC. Since liquid gasoline is injected in the MC during the intake stroke, it is likely that during the compression stroke liquid particles still survive, and the vapor fuel is not homogeneously distributed in the MC, yet. This implies that the mixture pushed inside the pre-chamber is mainly composed of air, rather than reflect the global λ level, especially at the beginning of the compression stroke. The model hence controls the composition of the incoming flux, also depending on the fuel evaporation rate and injection timing. In this way, a more accurate evaluation of λ inside the pre-chamber is foreseen.

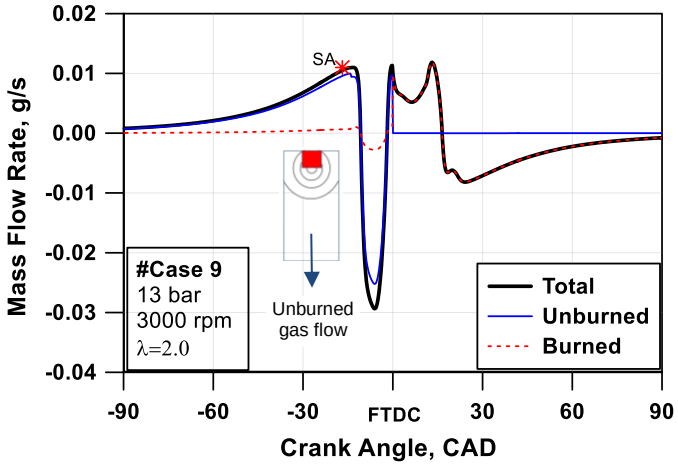

Figure 3.Instantaneous mass flow rate through the PC orifice.

Another assumption is introduced in the PC-MC mass exchange modeling: during the combustion process in the PC, it is expected that unburned gases firstly flow into the main chamber, while burned

gases arrive later, when the burning process in the PC goes towards its completion. Figure 3 better explains this model assumption by plotting the instantaneous mass flow rates through the orifice during the PC combustion. Burned gas flow rate (red dashed line) is only due to the presence of residuals in the PC, before the spark event. Unburned flux from PC to MC, usually characterized by a richer air/fuel composition, is able to enhance the very first phase of the burning process in the MC.

Burn-rate expression – The estimation of the burning rate in both PC and MC is, by all means, the most critical issue in the model. The starting point for combustion description is a quasi-dimensional fractal model, developed by the authors over last ten years [25]. The latter is based on a two-zone (burned and unburned) schematization, sensing both the combustion system geometry and the operating parameters. With reference to a standard SI engine, and according to the considered fractal approach, the burning rate can be written as:

$$\frac{dm_b}{dt} = \rho_u A_L S_T = \rho_u A_T S_L = \rho_u A_L S_L \frac{A_T}{A_L} = \rho_u A_L S_L \left(\frac{L_{\max}}{L_{\min}} \right)^{D_3 - 2} \quad (1)$$

ρ_u being the unburned gas density, A_L and A_T the area of the laminar and turbulent flame fronts, S_L and S_T the laminar and turbulent flame speeds. L_{max} and L_{min} are indeed the length scales of the maximum and minimum flame wrinkling, respectively, and D_3 the fractal dimension. D_3 is expressed through an empirical correlation as a function of the u'/S_L ratio, u' being the turbulence intensity. Eq. (1) is applied to either pre- and main-chamber, but a very different description of A_L, S_L, L_{max}, L_{min} and u' is specified.

Before discussing the combustion model details, it is important to underline that the theoretical background of the fractal model is based on the combustion regime occurring in a SI engine, falling in the wrinkled-corrugated flamelets domain. This may be not the case for the MC combustion process, since the laminar flame speed is low, due to the diluted mixture. As a consequence, the combustion regime moves toward the thickened wrinkled flamelets, where the thickness of the flame reaction zone may become larger than micro-eddies of Kolmogorov size, and Karlovitz number may assume values greater than unity. In a passive system, moreover, low flame speeds and reduced length scales substantially modify the combustion regime in the pre-chamber, too [13]. A stoichiometric combustion in the pre-chamber indeed most likely occurs in the conventional wrinkled-corrugated flamelets domain. In the light of these observations, the soundness of the theoretical basis of the fractal approach has to be case-by-case verified.

Turbulence – The estimation of L_{max}, L_{min} and u' is based on a in-house developed turbulence sub-model [26]. It belongs to the *K-k* family, and, in its latest version [27], also includes a balance equation for the tumble angular momentum. The model describes the energy cascade from the mean flow kinetic energy, *K*, to the turbulent kinetic energy, *k*, taking directly into account inlet and outlet mass flow rates through the valves. The turbulence sub-model is applied to both chambers and is here further extended to describe the turbulence production in the pre-chamber, induced by the incoming flow through the orifice along the compression stroke. Similarly, an additional turbulence production is considered in the main-chamber, as a consequence of the turbulent jets occurring when the burning process develops in the pre-chamber. A further source term is finally considered, to handle the intense turbulence production generated by the fuel injection in the pre-chamber. No ordered motions are presently modeled in the PC.

Following a well-assessed hierarchical 1D-3D approach [26], the tuning constants of turbulence sub-model are selected in order to fit the 3D-derived turbulent intensity profiles in both volumes. To this aim, preliminary 3D CFD analyses are carried out in motored conditions on the SCE engine at VKA. Figure 4 reports a comparison between the turbulence intensity computed by the 0D model and the one resulting from the mass-averaged turbulence intensity field in the 3D model, at each crank angle. The agreement is very satisfactory in the MC (continuous red line) during intake and compression phases, and in particular, close to the firing TDC, where the typical turbulence speed-up, due to the collapse of the tumble motion, occurs. Concerning the pre-chamber, 3D analysis provided data just before the FTDC. The PC turbulence (dashed red line) smoothly increases during the compression stroke, as a consequence of the incoming flow from the main volume. The PC turbulence peak is in good agreement with 3D outcomes. The 0D trend in the PC clearly highlights a turbulence increase at the BDC, where PC injection takes place. Moreover, looking at the zoomed view in Figure 4, two additional turbulence peaks are predicted by the 0D model. The first one, referring to the MC, is due to the turbulent jet coming from the PC, occurring towards the completion of the in-PC combustion. The second one, referring to the PC, verifies when the combustion takes place in the MC, and a reversed pressure difference induces once again an incoming flow inside the PC. Both these peaks are not visible in 3D data, since motored conditions have been considered.

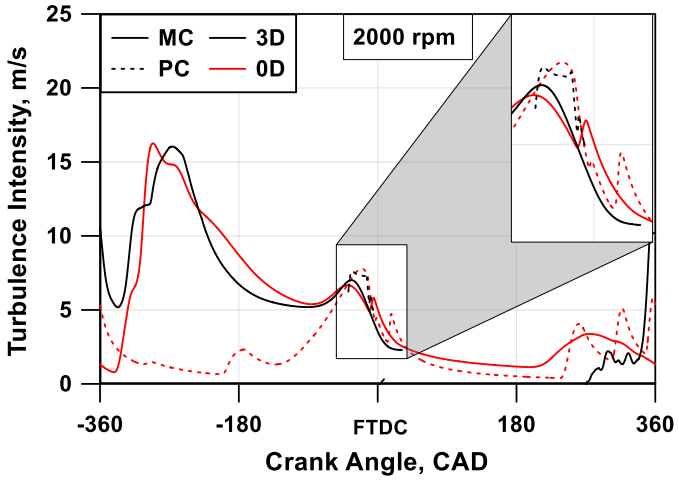

Figure 4. 0D/3D comparison of turbulence intensity in PC and MC.

Laminar flame area – For A_L estimation in Eq. (1), the classical assumption of a smooth spherically-shaped surface, centered on the spark-plug, can be adopted only for the pre-chamber. The corresponding flame area can be hence straightforwardly computed as the intersections between a sphere and the pre-chamber, which can be roughly schematized with a cylinder. In the main-chamber, indeed, the flame area development is much more complicated, since both a radial and an axial flame development is expected along each turbulent jet. Under the hypothesis of symmetrical jets, and assuming that the flame area mainly develops when turbulent jets have almost dissipated their initial kinetic energy [28], a simplified flame area assessment can be attempted. Following this idea, a fictitious ignition site is located along each turbulent jet in a mid-span position between the orifice and the cylinder walls. From each ignition site, spherical flames develop during time, until they intersect each other and with the combustion chamber walls. They finally collapse and fill the whole main-chamber volume. The above procedure is graphically explained in Figure 5, depicting the flame development in both the pre-chamber (in blue) and main-chamber (in red) during time.

With the above simplified schematization, it is possible to estimate the overall flame area, as a function of the radius for each single sphere, as displayed in Figure 6. Compared with a standard engine having the same displacement (no pre-chamber and with a centered spark plug), the overall flame area largely increases during the first combustion period. Initially, the flames propagating from each ignition site do not intersect each other. Later, indeed, the flame area rapidly decreases, due to flame-to-flame and flame-to-wall collisions. Figure 7 also reports the computed PC flame area.

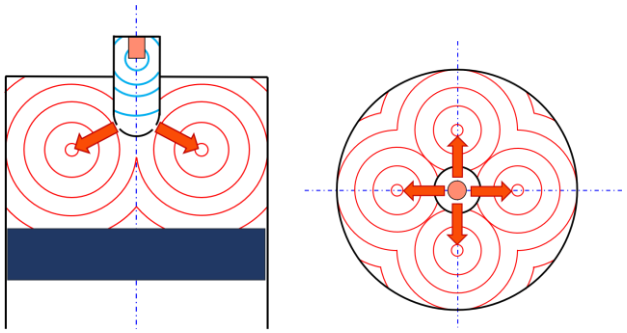

Figure 5. Frontal and upper view of a simplified schematization of the flame development in the PC and MC.

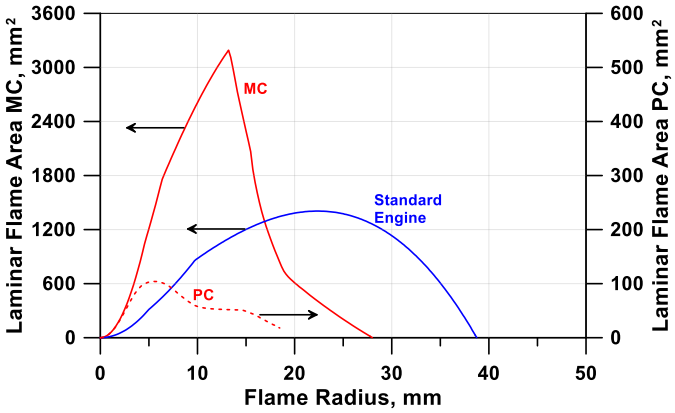

Figure 6. Laminar flame area comparison between a standard a divided-chamber engine against the flame radius.

While the PC flame area profile in Figure 6 is unique, since it does not depend on piston position, the one in main-chamber varies with the crank-angle. A look-up table can be however created once for a specified geometry, collecting flame areas in the MC at each piston position. The table is read at run-time, providing the time evolution of A_L to be included in Eq. (1). Typical trends of PC and MC laminar flame areas as function of the crank angle are depicted in Figure 7. Here, it is well evident that the burning process in the MC starts later than the one in the PC. The combustion start in the MC is predicted according to the flame radius in the PC. As soon as it overcomes a critical value, proportional to the PC cylinder height, the MC combustion is activated. A tuning constant is added to refine this critical value, in order to more precisely set the MC combustion start.

Laminar flame speed – For S_L estimation in Eq. (1), two correlations are utilized. For the main-chamber, where a RON98 gasoline is injected, a correlation developed within the EAGLE project at IFPEN is employed. It was built by using the kinetic scheme proposed in [29] and a TRF gasoline blend with the addition of ethanol. Although not of interest in the present study, the above correlation is also suitable for H_2-boosted combustions.

Since CNG fuel is injected in the pre-chamber, an additional laminar flame speed correlation is employed. The one proposed in [30] is coded in the model. However, it must be considered that, due to the mass exchanges, some vapor gasoline is also present in the pre-chamber and some methane may escape the pre-chamber during the injection, flowing into the main-chamber. For this reason, the employed correlation for pure gasoline and methane does not perfectly hold for the actual operation of this engine. However, a flame speed correlation for a gasoline-methane blend is not available at this stage of the research, and, in the following, the presence of pure gasoline and methane is assumed in the MC and PC, respectively.

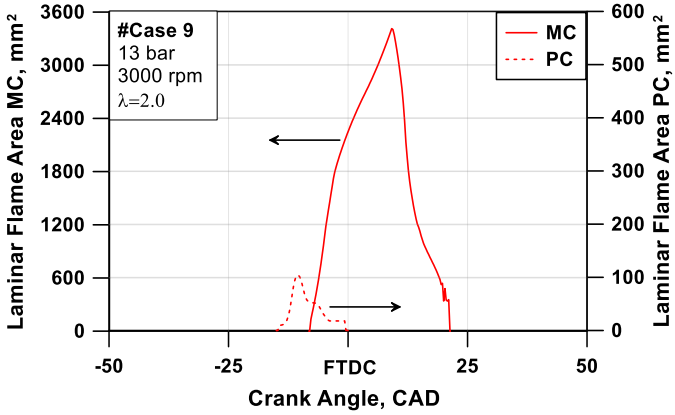

Figure 7. Laminar flame area for the PC and MC against the crank angle.

Turbulent flame speed – From eq. (1), it is easy to derive an expression for the turbulent flame speed, as:

$$S_T = S_L \left(\frac{L_{\max}}{L_{\min}} \right)^{D_3 - 2} \qquad (2)$$

In such an engine, the flame propagation in the MC, especially during the first stage, is also dependent on turbulent jet velocity [31]. As already pointed out, moreover, the richer air/fuel mixture escaping the PC during early combustion progress is expected to enhance the first phase of the burning progress in the main-chamber. In order to include these dependencies in the model, a modified flame speed estimation is proposed. First, a velocity scale inside the PC, v_p, is computed, based on the instantaneous mass flow rate through the orifice, the axial PC area and a tunable scale factor, x_v. This velocity increases during the PC combustion, reaches a maximum value, $v_{p,max}$, and then rapidly falls, becoming negative when the MC combustion takes place. The jet tip in the MC, which is assumed to scale with velocity in the pre-chamber, is indeed expected to still propagate with a relaxing velocity, v_{tip}. This last is assumed to decay because of the shear resistance arising from the interaction of the jet with unburned mixture in the MC. It is estimated by Eq. (3), imposing a decay in a characteristic time scale, τ, assigned as a model constant:

$$v_{tip} = v_{p,\max} e^{-t/\tau} \qquad (3)$$

An overall turbulent flame speed, $S_{T,ov}$, is then estimated by combining the S_T, derived from Eq. (2), with the relaxed tip velocity:

$$S_{T,ov} = \max\left(S_T, v_{tip} \right) \qquad (4)$$

The latter is finally introduced in the modified burning rate expression:

$$\frac{dm_b}{dt} = \rho_u A_L S_{T,ov} \qquad (5)$$

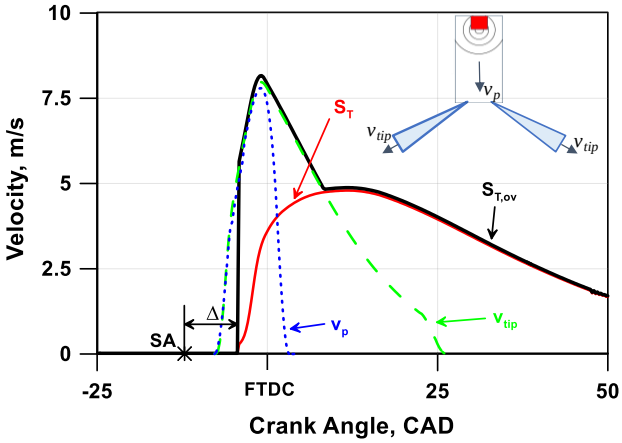

Figure 8. Characteristic velocities for overall turbulent flame speed estimation.

In Figure 8, representative velocities v_p, v_{tip}, S_T and $S_{T,ov}$ are depicted to better explain the model logic. It is evident that the flame speed correction is only active during the first part of the combustion progress in the main-chamber. The delay, Δ, between SA in the pre-chamber and first S_T and $S_{T,ov}$ estimation in the MC corresponds to time required by the flame to travel within the PC.

SACI regime – Before assessing the approach accuracy, another model feature is here introduced. Figure 9 reports the experimental pressure cycle in both pre- and main- chambers, obtained in Case #4. The in-cylinder pressure is also processed to derive the related burn rate. Looking at its shape, it is well evident a burn rate increase phased with the maximum pressure in the PC. At this time, the turbulent jets are entering the MC, with a fast initial MC burn rate, confirming the assumptions behind the previously discussed expression of the overall flame speed, $S_{T,ov}$. Later during the process, the experimental burn rate continuously increases, determining a change of concavity in the pressure cycle. This behavior resembles the burn rate profiles occurring in a Spark-Assisted Compression-Ignition (SACI) combustion regime [32]. In this regime, the presence of intermediate species ahead of the flame, together with the release of some heat in the unburned zone (cool flames), is responsible for flame acceleration. This specific burn rate shape has been detected in different operating conditions, and particularly at high load and very lean mixture, coupled with high intake boosting. Recalling the experimental MFB_{50} values listed in Table 2, it seems reasonable that the engine is operating at the boundary between a deflagration regime and a spontaneous ignition front regime. In the former, the reaction front locally propagates at the laminar flame speed, while in the latter, the apparent propagation of the reaction is much higher, since it results from a cascade of ignition events [33].

To model these two distinct phases, the thermodynamic state in the unburned gas zone is computed considering the heat release arising from auto-ignition reactions. As done for some refined knock modeling, a chemical kinetic scheme is solved at each crank angle in the unburned zone. The kinetic scheme adopted here was developed by Andrae et al. [34] and modified to also add NO and ethanol oxidation sub-mechanisms. The overall scheme, constituted by 5 elements, 185 species and 937 reactions, is solved with reference to a four-component gasoline surrogate, including iso-octane, n-heptane, toluene and ethanol. The mole fractions of the components in the fuel surrogate are chosen to mimic an oxygenated European gasoline. The above methodology allows to estimate an increased unburned gas zone temperature, depending on the activation of low- and high-temperature auto-ignition reactions. The enhanced unburned temperature is finally utilized in the laminar flame speed correlation.

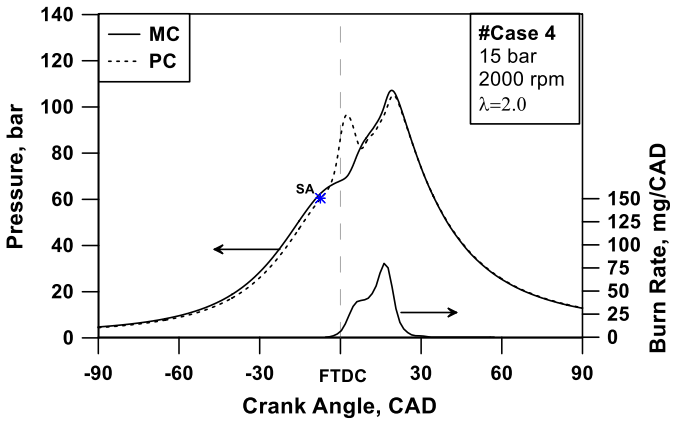

Figure 9. Experimental in-cylinder pressure cycle and burn rate at 2000 rpm, 15 bar IMEP and λ=1.0.

Figure 10 puts into evidence that the laminar flame speed in the MC, red line, starting from very low values due to the mixture dilution, during time rapidly increases when auto-ignition reactions in the unburned zone are considered to mimic the SACI regime. Flame speeds higher than 2 m/s are estimated, attaining levels which were theoretically predicted in some studies [32,33] about the SACI combustion regimes.

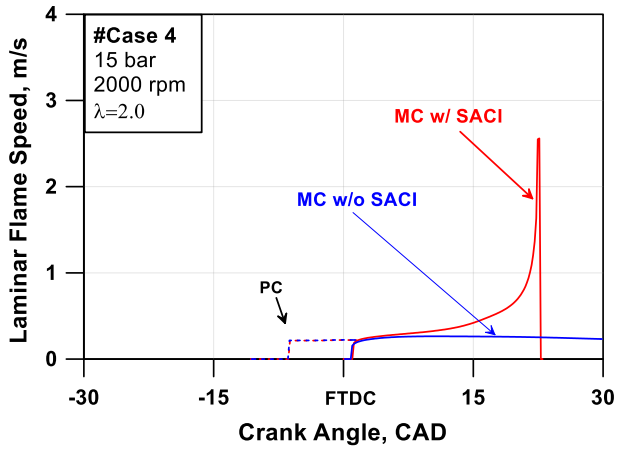

Figure 10. Laminar flame speed in the MC (w/ and w/o SACI regime) and PC.

Correspondingly, the estimated burn rate and pressure cycle in Figure 11 move towards the related experimental data, otherwise a very poor agreement is obtained. Results show that the updated relation for turbulent flame speed, Eq. (4), is able to qualitatively reproduce the initial knee of the burn rate. It then sharply increases few crank angles later than measurements. The disagreement can be attributed to some problems in the prediction of temperature levels ahead of the flame, which, in turn, can be related to inaccuracies of the heat exchange sub-model, or due to the presence of some temperature stratification in the unburned gas, which cannot be taken into account in a 0D model. In any case, the obtained results seem to confirm that a quasi-SACI regime is actually occurring in the tested engine.

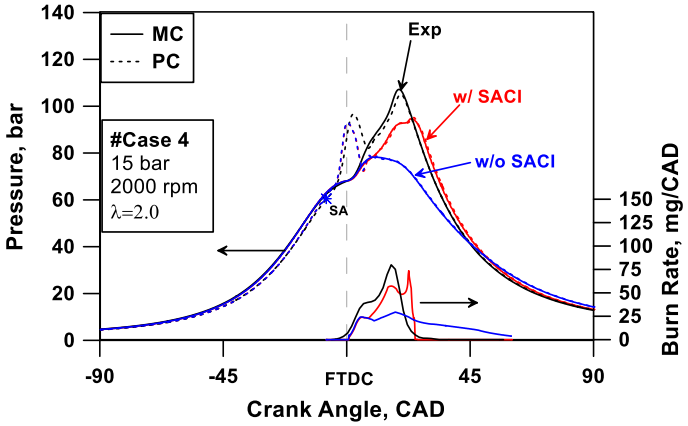

Figure 11. Experimental/numerical comparison of in-cylinder pressure cycle and burn rate at 2000 rpm, 15 bar IMEP, λ=2.0 w/ and w/o SACI regime.

Model Tuning – The described quasi-dimensional model requires, as usual, some tuning. The original version of the fractal combustion model, suitable for a standard SI engine, includes 3 tuning constants. They act respectively on the flame wrinkling extent, on the transition between an initially-laminar and a fully-turbulent combustion, and on the combustion tail. The present pre-chamber version adds some more constants to adjust the overall turbulent flame speed and the MC combustion start. The model tuning is carried out to reproduce as good as possible the pressure traces in both PC and MC, partly following a methodology reported in previous works of the authors [35], and partly through a trial-and-error procedure. One single set of tuning constants has been determined by this procedure and it has been used for all the operating points simulated.

Engine model validation

The model is validated through numerical/experimental comparisons in the 13 operating points listed in Table 2. Three engine speeds are considered, namely 2000, 3000 and 4000 rpm, and λ values between 1.0 and 2.4. To get the maximum numerical/experimental congruence, the same boundary conditions as the experiments have been assigned in the simulations, which are the spark timing, intake and exhaust pressure and temperature, and mass of injected gasoline and CNG.

The first stage of the model validation is focused on the global engine performance. The IMEP values, as depicted in the right side of Figure 12, are quite correctly predicted, although a certain systematic model overestimation is evident. This is probably due to an underprediction of the heat losses. The same kind of disagreement, in Figure 12 on the left, characterizes the engine efficiency trend. The model well detects the improvement of the engine efficiency when λ increases.

The model capability in reproducing the air flow rate is shown in Figure 13. The satisfactory agreement demonstrates an accurate schematization of the intake and exhaust pipe geometry and a proper specification of the valve flow coefficients. A certain underestimation, up to 2-3 g/s, is visible, especially at growing λ values. An additional confirmation of the correct geometrical model schematization is shown in Figure 14, which shows the numerical/experimental comparison of the PC pressure profiles in a representative operating condition. The model demonstrates to correctly describe the local pressure peak induced by the PC injection, and the amplitude and frequency of the oscillation during the exhaust phase. Since the spark advance is imposed in the simulations, the combustion model reliability is performed by the numerical/experimental comparison of the MFB_{50} values (Figure 15).

Additional verifications about the combustion modelling concern the combustion characteristic angles ($MFB_{0\text{-}10}$ and $MFB_{10\text{-}90}$ in Figure 16) and the pressure peaks (level and phasing in Figure 17) inside the pre-chamber and main-chamber.

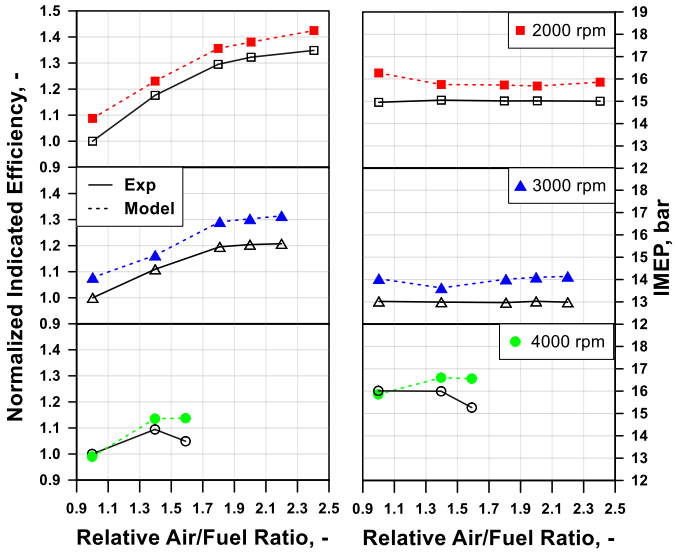

Figure 12. Numerical/experimental normalized indicated efficiency (a) and IMEP (b) assessment for different air/fuel ratios and engine speeds.

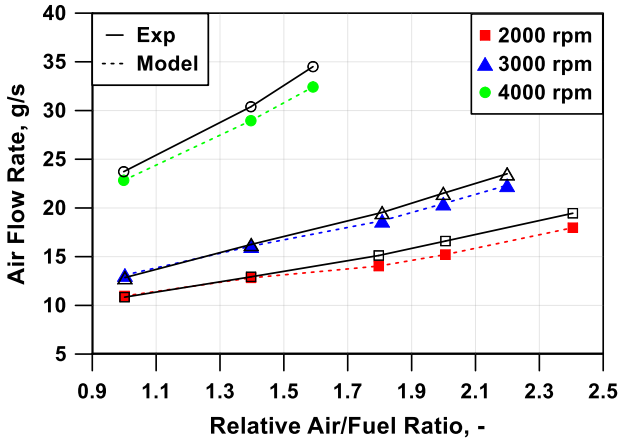

Figure 13. Numerical/experimental air flow rate assessment for different air/fuel ratios and engine speeds.

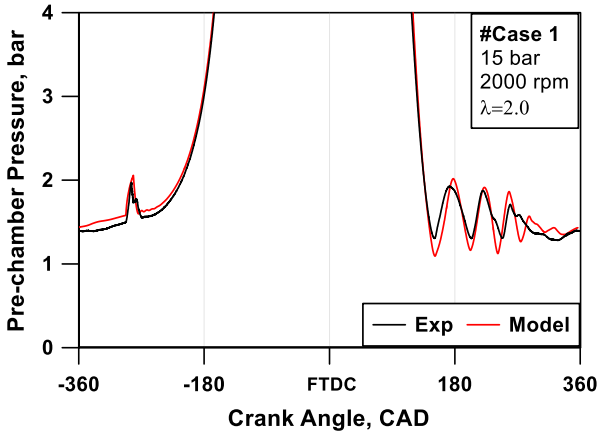

Figure 14. Experimental/numerical comparison of in-cylinder low pressure cycles at 2000 rpm, 15 bar IMEP, λ=2.0.

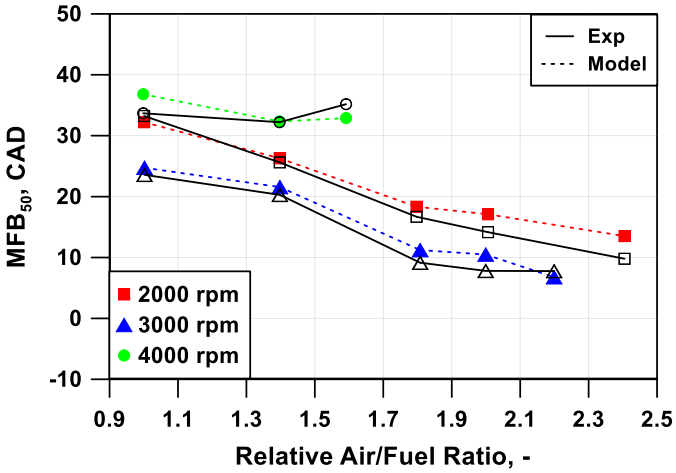

Figure 15. Numerical/experimental MFB_{50} assessment for different air/fuel ratios and engine speeds.

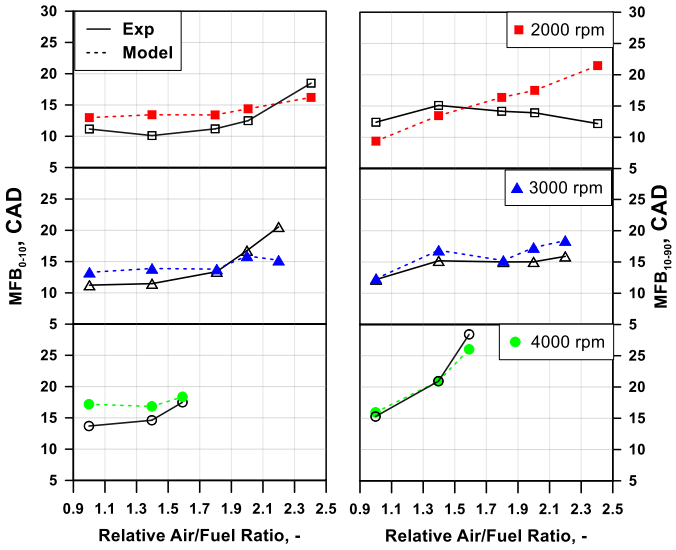

Figure 16. Numerical/experimental MFB_{0-10} and MFB_{10-90} assessments for different air/fuel ratios and engine speeds.

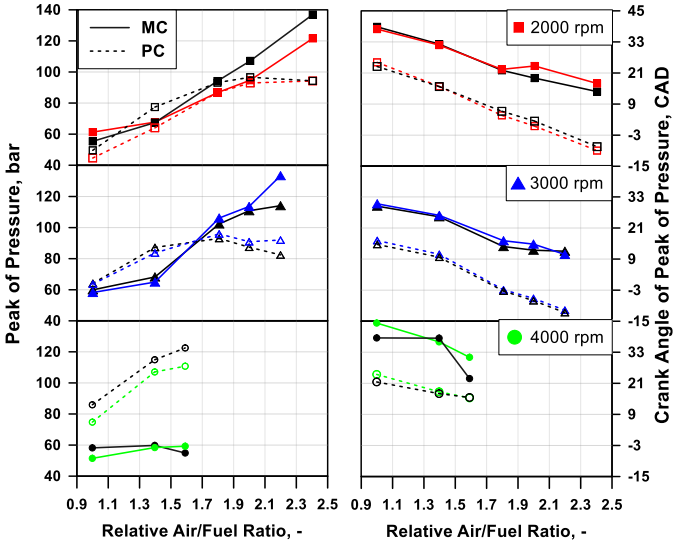

Figure 17. Numerical/experimental comparison of pressure peaks and related locations in the MC and PC for different air/fuel ratios and engine speeds.

As pointed out in Figure 15, at least for 2000 and 3000 rpm, the experimental MFB_{50} is advanced when the mixture is leaned, according to the spark timing selection reported in Table 2. The possibility of optimizing the combustion phasing is due to the lower knock propensity of leaner mixtures. This also partially explains the engine efficiency increase for higher λ, shown in Figure 12 left. The model reproduces the experimental MFB_{50} trends with a very satisfactory accuracy for all the considered speeds and λ levels.

To better analyze the combustion evolution, the numerical/experimental comparisons of MFB_{0-10} and MFB_{10-90} can be observed (Figure 16). Differently from a conventional engine, characterized by a consistent combustion lengthening at rising relative air/fuel ratios, here this behavior is much less evident. The combustion duration (MFB_{10-90}) is in fact almost insensitive to the mixture quality, excepting at 4000 rpm. At this speed more critical knock conditions occur and a very delayed MFB_{50} is established whichever is the λ (Table 2 and Figure 15). Consequently, the combustion develops during the expansion stroke and long burn durations verify.

Those characteristics are quite accurately captured by the model, without the need of any tuning adjustment. The main errors concern the computation of the leanest operating points at 2000 rpm, where combustion duration is much longer than experiments.

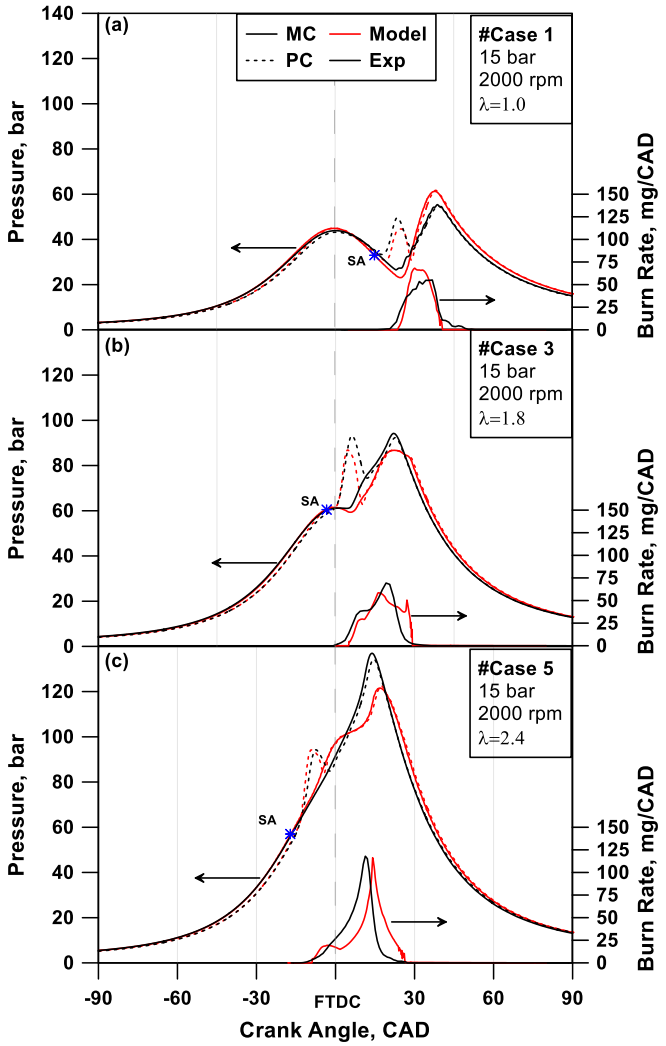

Figure 18. Experimental/numerical comparison of in-cylinder pressure cycle and burn rate at 2000 rpm, 15 bar IMEP, (a) λ=1.0, (b) λ=1.8, (c) λ=2.4.

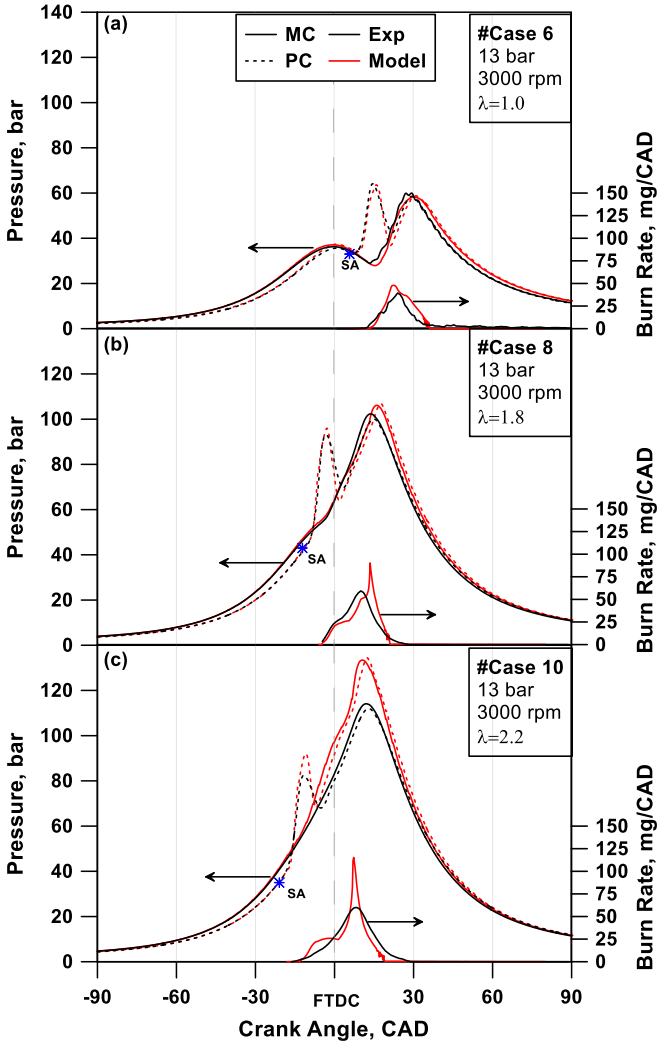

Figure 19. Experimental/numerical comparison of in-cylinder pressure cycle and burn rate at 3000 rpm, 13 bar IMEP, (a) λ=1.0, (b) λ=1.8, (c) λ=2.2.

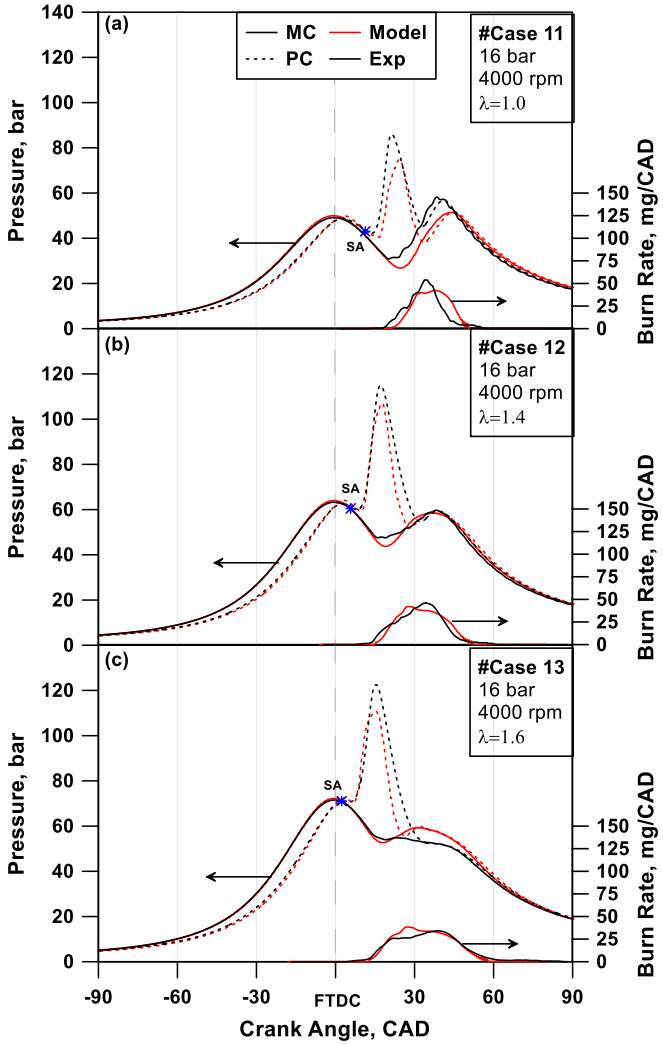

Figure 20. Experimental/numerical comparison of in-cylinder pressure cycle and burn rate at 4000 rpm, 16 bar IMEP, (a) λ=1.0, (b) λ=1.4, (c) λ=1.6.

The correct combustion description reflects on the peak pressure prediction, depicted in Figure 17 on the left. The observed peak pressure increases at mixture leaning is due to the need of boosting to maintain the same engine load. The model also well forecasts the peak pressure position, as shown on the right side of Figure 17.

A further insight in the model reliability is proved by the numerical/experimental comparisons of the in-cylinder pressure cycles and of the related burn rates for λ sweeps at 2000, 3000 and 4000, high load, depicted in Figure 18, Figure 19 and Figure 20, respectively. The measured MC pressure cycles are represented by continuous black lines, while the correspondent PC traces with dashed black ones. The red lines (continuous and dashed) refer to the numerical outcomes. The figures highlight that, on one hand, the mixture leaning allows to advance the spark, but on the other hand, an increased boosting is necessary to maintain the load, as underlined by the pressure level during the compression phases. The agreement between numerical/experimental pressure trends is quite satisfying, in terms of global shape, timing and peak levels in both MC and PC. Moreover, the model correctly describes the increasing PC/MC pressure difference at growing engine speed, thanks to a proper selection of the orifice discharge coefficient. Model consistency to handle very lean conditions is related to the introduction in the model of the description of the SACI combustion mode.

This is stressed in the operating points with λ values higher than 1.8, as shown in Figure 18c and Figure 19b-c. The model is able to perceive and reproduce this occurrence, not present in both experimental data and numerical outcomes for lower λ levels. These results can be considered an indirect confirmation of the modelling assumptions about the SACI combustion regime.

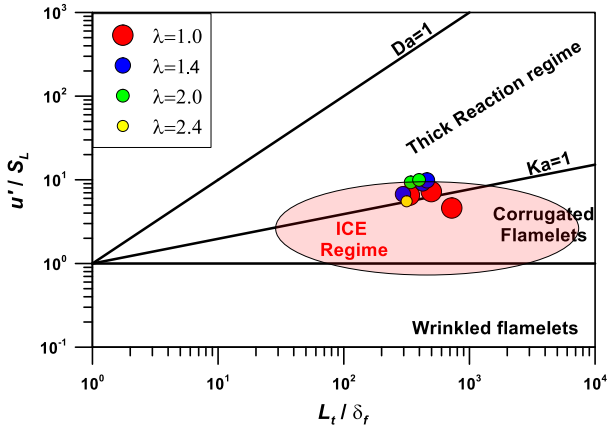

Figure 21. Borghi diagram of computed combustion regime in the MC at MFB_{50} for various λ values.

As a final check, the combustion regime is evaluated at the MFB_{50} crank-angle in the MC, for most of the analyzed operating conditions (Figure 21). As expected, at high excess-air the combustion regime moves towards the thick reaction zone, as a consequence of the reduced laminar flame speed. The same does not happen at the leanest λ of 2.4, since the presence of a quasi-SACI regime is responsible for a relevant flame acceleration (Figure 10 and Figure 18). Most of the analyzed conditions, however, still lie close to the conventional ICE regime, which justifies the adoption of the proposed fractal model.

Conclusions

In this work, a quasi-dimensional model for a SI engine, equipped with an active pre-chamber is presented and validated by a detailed numerical/experimental assessment. Experiments are carried out at the VKA of the RWTH Aachen University, in a single-cylinder divided-chamber engine, fueled with CNG in the pre-chamber and liquid gasoline in the main-chamber. Among the collected data, 13 representative operating points are selected, characterized by different engine speeds and λ values up to 2.4, at constant load. The modelling approach for the description of the basic phenomena occurring in the active pre-chamber engine arises from a fractal combustion model developed by the authors in the last years for conventional SI engines. Both turbulence and combustion sub-models are modified to handle a divided chamber engine architecture. The turbulence and the burn rate enhancement due to burned gas jets is considered in the updated model. Moreover, a new formulation for the estimation of the laminar area in the MC is proposed, based on the development of multiple flames centered in fictitious ignition sites. Another key feature of the model is the attempt to describe a SACI combustion regime likely occurring at very lean conditions. To this aim, a laminar flame speed enhancement is introduced, promoted by the activation of low-temperature auto-ignition reactions in the unburned gas.

The above model is embedded in a 1D code and is verified against the experimental pressure traces in both PC and MC. Global engine performance is also compared with measurements. The model proves a good capability in predicting the air flow rate, efficiency and IMEP, even for very lean mixtures. Concerning the pressure traces and the related burn rate profiles, the agreement between numerical and experimental data is satisfactory. The model consistency is finally verified checking the combustion regime on the Borghi diagram. It is not worthless to underline that the presented numerical results are obtained without modifying the tuning constants of the model. This is not obvious, considering the variations of the engine speed, mainly perceived by the turbulence sub-model, and of the mixture quality, principally taken into account by the laminar flame speed correlation. A high model reliability is hence demonstrated in considering the physics behind such complex and still not completely understood combustion modality. The model prediction of NO_X emission will be verified against the experimental data in future activities.

Contact information

References

1. Saber, A., Venayagamoorthy, G., "Plug-in vehicles and renewable energy sources for cost and emission reductions," *IEEE Transactions on Industrial electronics* 58.4 1229-1238,2011, doi:10.1109/TIE.2010.2047828.
2. Khaligh, A., Li, Z., "Battery, ultracapacitor, fuel cell, and hybrid energy storage systems for electric, hybrid electric, fuel cell, and plug-in hybrid electric vehicles: State of the art," *IEEE transactions on Vehicular Technology*, *59*(6), 2806-2814, 2010, doi:10.1109/TVT.2010.2047877.
3. De Bellis, V., Bozza, F., Siano, D., Gimelli, A., "Fuel consumption optimization and noise reduction in a spark-ignition turbocharged VVA engine," *SAE International Journal of Engines*,*6*(2), 1262-1274, 2013, doi:10.4271/2013-01-1625.
4. Roberts, M., "Benefits and Challenges of Variable Compression Ratio (VCR)," SAE Technical Paper 2003-01-0398, 2003, doi:10.4271/2003-01-0398.
5. Francqueville, L., Michel, J., "On the Effects of EGR on Spark-Ignited Gasoline Combustion at High Load," *SAE Int J Engines* 7(4):1808-1823, 2014, doi:10.4271/2014-01-2628.
6. Hoppe, F., Thewes, M., Baumgarten, H., Dohmen, J., "Water injection for gasoline engines: Potentials, challenges, and solutions," *International J of Engine Research* 17(1):86-96, 2016, doi: 10.1177/1468087415599867.
7. Germane, G., Wood, C., Hess, C., "Lean Combustion in Spark-Ignited Internal Combustion Engines - A Review," SAE Technical Paper 831694, 1983, doi: 10.4271/831694.
8. Bozza, F., De Bellis, V., Teodosio, L., Tufano, D., Malfi, E., "Techniques for CO_2 Emission Reduction over a WLTC. A Numerical Comparison of Increased Compression Ratio, Cooled EGR and Water Injection," SAE Technical Paper 2018-37-0008, 2018, doi:10.4271/2018-37-0008.
9. Rapp, V., Killingsworth, N., Therkelsen, P., et al., "Lean Combustion, 2nd Edition," Lean-Burn Internal Combustion Engines, Elsevier,2016, 111-146. doi:10.1016/C2013-0-13446-0
10. Heywood, J., B., *Internal combustion engine fundamentals*," Vol. 930 (New York, Mcgraw-Hill, 1988), ISBN: 007028637X.
11. Sens, M., Binder, E., Benz, A., Kramer, L., at all. "Pre-chamber ignition as a Key Technology for Highly Efficient SI Engines-New Approaches and Operating Strategies," 39th International Vienna Motor Symposium, Apr. 2018.
12. Roethlisberger, R., Favrat, D., "Comparison between direct and indirect (prechamber) spark ignition in the case of a cogeneration natural gas engine, part I: engine geometrical parameters," *Applied Thermal Engineering*, 22(11), 1217-1229, 2002, doi: 10.1016/S1359-4311(02)00040-6.
13. Xu, G., Wright, Y., Schiliro, M., Boulouchos, K., "Characterization of combustion in a gas engine ignited using a small un-scavenged pre-chamber," *International Journal of Engine Research*, 2018, doi: 10.1177/1468087418798918.
14. Mueller, C., Morcinkowski, B., Habermann, K., Uhlmann, T., Schernus, C. "Development of a pre-chamber for spark ignition engines in vehicle applications," 4th International Conference on Ignition Systems for Gasoline Engines, Dec. 2018.
15. Jamrozik, A., "Lean combustion by a pre-chamber charge stratification in a stationary spark ignited engine," *Journal of Mechanical Science and Technology*, 29(5):2269-2278, 2015, doi: 10.1007/s12206-015-0145-7.
16. Toulson, E., Schock, H., Attard, W., "A Review of Pre-Chamber Initiated Jet Ignition Combustion Systems," SAE Technical Paper 2010-01-2263, 2010, doi: 10.4271/2010-01-2263.
17. Lumsden, G., Watson, H., "Optimum Control of an S.I. Engine with a λ=5 Capability," SAE Technical Paper 950689, 1995, doi: 10.4271/950689.
18. Schumacher, M., Wensing, M., "A Gasoline Fuelled Pre-Chamber Ignition System for Homogeneous Lean Combustion

Processes," SAE Technical Paper 2016-01-2176, 2016, doi:10.4271/2016-01-2176.
19. Jamrozik, A., Tutak, W., Kociszewski, A., Sosnowski, M., "Numerical simulation of two-stage combustion in SI engine with prechamber," *Applied Mathematical Modelling*, 37(5), 2961-2982, 2013, doi: 10.1016/j.apm.2012.07.040.
20. Shah, A., Tunestål, P., Johansson, B., "CFD Simulations of Pre-Chamber Jets' Mixing Characteristics in a Heavy Duty Natural Gas Engine," SAE Technical Paper 2015-01-1890, 2015, doi: 10.4271/2015-01-1890.
21. Gentz, G., Thelen, B., Litke, P., Hoke, J., Toulson, E., "Combustion visualization, performance, and CFD modeling of a pre-chamber turbulent jet ignition system in a rapid compression machine," *SAE International Journal of Engines*, 8(2), 538-546, 2015, doi: 10.4271/2015-01-0779.
22. Bardis, K., Xu, G., Kyrtatos, P., Wright, Y. et al., "A Zero Dimensional Turbulence and Heat Transfer Phenomenological Model for Pre-Chamber Gas Engines," SAE Technical Paper 2018-01-1453, 2018, doi:10.4271/2018-01-1453.
23. Cruz, I., Alvarez, C., Teixeira, A., Valle, R., "Zero-dimensional mathematical model of the torch ignited engine," *Applied Thermal Engineering*, 103, 1237-1250, 2016, doi: 10.1016/j.applthermaleng.2016.05.017.
24. Spindt, R., "Air-Fuel Ratios from Exhaust Gas Analysis," SAE Technical Paper 650507, 1965, doi: 10.4271/650507.
25. De Bellis, V., Severi, E., Fontanesi, S., Bozza, F., "Hierarchical 1D/3D approach for the development of a turbulent combustion model applied to a VVA turbocharged engine. Part II: combustion model," *Energy Procedia*, 45: 1027-1036, 2014, doi: 10.1016/j.egypro.2014.01.108.
26. De Bellis, V., Bozza, F., Fontanesi, S., Severi, E. et al., "Development of a Phenomenological Turbulence Model through a Hierarchical 1D/3D Approach Applied to a VVA Turbocharged Engine," *SAE Int. J. Engines* 9(1):506-519, 2016, doi:10.4271/2016-01-0545.
27. Bozza, F., Teodosio, L., De Bellis, V., Fontanesi, S. et al., "Refinement of a 0D Turbulence Model to Predict Tumble and Turbulent Intensity in SI Engines. Part II: Model Concept, Validation and Discussion," SAE Technical Paper 2018-01-0856, 2018, doi:10.4271/2018-01-0856.
28. Mastorakos, E., Allison, P., Giusti, A., De Oliveira, P., Benekos, S., Wright, Y., Boulouchos, K, "Fundamental Aspects of Jet Ignition for Natural Gas Engines," *SAE International Journal of Engines*, doi:10.4271/2017-24-0097.
29. Bounaceur, R., Herbinet, O., Fournet, R., Glaude, P. et al., "Modeling the Laminar Flame Speed of Natural Gas and Gasoline Surrogates," SAE Technical Paper 2010-01-0546, 2010, doi:10.4271/2010-01-0546.
30. Amirante, R., Distaso, E., Tamburrano, P., Reitz, R. D., "Laminar flame speed correlations for methane, ethane, propane and their mixtures, and natural gas and gasoline for spark-ignition engine simulations," *International Journal of Engine Research*, 18(9), 951-970, 2017, doi: 10.1177/1468087417720018.
31. Alvarez, C., Couto, G., Roso, V., Thiriet, A., Valle, R., "A review of prechamber ignition systems as lean combustion technology for SI engines," *Applied Thermal Engineering*, 128: 107-120, 2018, doi: 10.1016/j.applthermaleng.2017.08.118.
32. Martz, J., Kwak, H., Im, H., Lavoie, G., Assanis, D., "Combustion regime of a reacting front propagating into an auto-igniting mixture," *Proceedings of the Combustion Institute*, 33(2), 3001-3006, 2011, doi: 10.1016/j.proci.2010.07.040.
33. Martz, J., Lavoie, G., Im, H. Middleton, R., Babajimopoulos, A., Assanis, D., "The propagation of a laminar reaction front during end-gas auto-ignition," *Combustion and Flame*, 159(6), 2077-2086, 2012, doi: 10.1016/j.combustflame.2012.01.011.
34. Andrae, J., Kovács, T., "Evaluation of Adding an Olefin to Mixtures of Primary Reference Fuels and Toluene to Model the Oxidation of a Fully Blended Gasoline," *Energy & Fuels*, 30(9), 7721-7730, 2016, doi: 10.1021/acs.energyfuels.6b01193.
35. De Bellis, V., Bozza, F., Tufano, D., "A Comparison Between Two Phenomenological Combustion Models Applied to Different SI Engines," SAE Technical Paper 2017-01-2184, 2017, doi:10.4271/2017-01-2184.

Acknowledgements

"This project has received funding from the European Union's Horizon 2020 research and innovation programme under grant agreement No 724084"

Acronyms

0D-1D-3D	Zero-One-Three-dimensional
AFTDC	After firing top dead center
BDC	Bottom dead center
CAD	Crank angle degree
CFD	Computational fluid dynamics
CNG	Compressed natural gas
DI	Direct injection
EGR	Exhaust gas recirculation
HEV	Hybrid electric vehicle
FTDC	Firing top dead center
ICE	Internal combustion engine
IMEP	Indicated mean effective pressure
MC	Main-chamber
MFB	Mass fraction burned
PC	Pre-chamber
RON	Research Octane Number
SA	Spark advance
SACI	Spark assisted compression-ignition
SCE	Single cylinder engine
SI	Spark ignition
TRF	Toluene reference fuel

Symbols

A_L, A_T	Laminar / turbulent flame area
Da	Damköhler number
k	Turbulent kinetic energy
K	Mean flow kinetic energy
Ka	Karlovitz number
L_{min}, L_{max}	Minimum / maximum flame front wrinkling scale
L_t	Turbulence integral length scale
m	Mass
S_L, S_T	Laminar / turbulent flame speed
$S_{T,ov}$	Overall turbulent flame speed
t	Time
u'	Turbulence intensity
v_p, $v_{p,max}$	Velocity scale in pre-chamber and related max value
v_{tip}	Velocity of jet tip in main-chamber
x_v	Velocity scale multiplier

Greeks

ε	Dissipation rate
λ	Relative air/fuel ratio
ρ	Density
τ	Characteristic time delay for velocity jet tip
δ_f	Flame thickness

Subscripts

10 / 50 / 90	Referring to 10 / 50 / 90% of mass fraction burned
b	Burned
u	Unburned